Optical free-carrier generation in silicon nano-waveguides at 1550 nm

Cite as: Appl. Phys. Lett. **112**, 251104 (2018); https://doi.org/10.1063/1.5023589
Submitted: 25 January 2018 . Accepted: 06 June 2018 . Published Online: 19 June 2018

Andres Gil-Molina, Ivan Aldaya, Julián L. Pita, Lucas H. Gabrielli, Hugo L. Fragnito, and Paulo Dainese

Optical free-carrier generation in silicon nano-waveguides at 1550 nm

Andres Gil-Molina,[1,2,a)] Ivan Aldaya,[1,3,a)] Julián L. Pita,[2] Lucas H. Gabrielli,[2] Hugo L. Fragnito,[1,4] and Paulo Dainese[1,b)]
[1]*Gleb Wataghin Physics Institute, University of Campinas, Campinas-SP 13083-859, Brazil*
[2]*School of Electrical and Computer Engineering, University of Campinas, Campinas-SP 13083-852, Brazil*
[3]*Campus São João da Boa Vista, State University of São Paulo (UNESP), SP 13876-750, Brazil*
[4]*MackGraphe, Mackenzie Presbyterian University, São Paulo-SP 01302-907, Brazil*

(Received 25 January 2018; accepted 6 June 2018; published online 19 June 2018)

We report on time-resolved pump and probe characterization of linear and nonlinear optical generation of free carriers in a silicon strip nano-waveguide at the 1550 nm communication band. Analytical expressions were developed to extract the carrier density averaged along the waveguide length from the measured free-carrier absorption for different input pump power levels. This allows us to discriminate the contributions from two-photon absorption (TPA) and single-photon absorption (SPA), obtaining TPA and SPA coefficients of (1.5 ± 0.1) cm/GW and (1.9 ± 0.1) m^{-1}, respectively. Our results reveal that the effective TPA within the waveguide is higher than the value reported for bulk silicon. In addition, we find that for the waveguide under test, the carrier generation via SPA plays an important role up to ~300 mW, and therefore, it must be taken into account to correctly assess free-carrier effects in silicon photonic devices. *Published by AIP Publishing.* https://doi.org/10.1063/1.5023589

Free carriers have been identified as a critical factor in silicon photonics, giving rise to free-carrier absorption (FCA) and free-carrier dispersion (FCD).[1] These effects are especially important in strip waveguides, since free-carriers cannot diffuse out of the optical modal region. In many cases, the presence of free-carriers degrades the system performance, increasing losses and, for example, reducing parametric[2] and Raman net gain.[3] In addition, the generation and recombination of free carriers lead to self-heating that can further impact the behavior of resonant cavities.[4,5] Both FCA and FCD, however, may also be exploited to control light within the silicon structure.[6,7] Consequently, the accurate characterization of carrier dynamics is essential either to identify the operation limits of a certain device or to take advantage of it to develop novel applications. This is particularly important at wavelengths around 1550 nm, where most modern optical communication systems operate.

In nano-scale waveguides, carrier dynamics is governed by the interplay between carrier generation and recombination. Specifically, in strip waveguides where electrical carrier injection is difficult, the free-carriers are mainly generated by optical means.[3,8] Given the 1.12 eV bandgap of silicon, at 1550 nm, optical generation is usually attributed to two-photon absorption (TPA). Even if this assumption is accurate for high-power operation, single-photon absorption (SPA) due to intra-bandgap states ascribed to factors such as dopant concentration of silicon, crystalline defects, impurities diffused during the etching process, and surface states at the interface between silicon and oxide has been observed at low and medium power levels.[9–11] It is, therefore, important to identify each contribution and quantify them in terms of the input optical power. On the one hand, nonlinear carrier generation via TPA has been extensively analyzed, first in bulk silicon[12–14] and then in waveguides,[15–19] showing an enhancement of the TPA coefficient in sub-wavelength guiding structures. This enhancement has been observed by Liu *et al.*[19] at mid-infrared wavelengths in waveguides with cross-sections of 600 nm × 220 nm; however, it has not been analyzed at the 1550 nm communications window. On the other hand, linear carrier generation through SPA has been used to build waveguide detectors[9] and light monitoring devices[10] and has been recently analyzed by Grillanda and Morichetti.[11] In these previous works, the effect of SPA has been characterized by measuring the generated photocurrent,[9] the waveguide electrical conductance,[10] or the attenuation coefficient[11] as a function of the input power. This however does not give a direct characterization of the more fundamental SPA absorption coefficient, as the attenuation itself depends on other parameters such as the carrier lifetime and the TPA coefficient.

The characterization of the enhanced-TPA at 1550 nm and a direct measurement of the SPA coefficient in nano-waveguides are therefore lacking. In this letter, we *simultaneously* measured both the linear and nonlinear optical free-carrier generation at 1550 nm in a typical single-mode strip silicon waveguide. We use a method based on time-resolved pump-and-probe that exploits the different time scales of free-carrier generation and recombination processes to measure the generated free-carriers in terms of the input pump power. This approach, alongside with developed analytical expressions, allows us to accurately discriminate the contributions of TPA and SPA.

We analyzed a 2.4 mm-long silicon-on-insulator (SOI) waveguide with silica cladding and a cross-section of 450 nm × 220 nm. The waveguide was fabricated at imec/Europractice using optical lithography and inductively coupled plasma—reactive ion etching. Two grating couplers were placed at both ends for input and output light coupling. We used two additional samples with lengths of 5.9 mm and

[a)]A. Gil-Molina and I. Aldaya contributed equally to this work.
[b)]Electronic mail: dainese@ifi.unicamp.br.

30 mm to measure coupling and linear propagation losses by performing linear regression of low-power transmittance, resulting in 1.4 dB/cm propagation loss and 3.7 dB coupling loss from grating to cleaved fiber. The carrier generation characterization in the waveguide under test was performed using the pump and probe experimental setup described by Aldaya *et al.*[20] A strong pulsed pump generates free-carriers (through both SPA and TPA), which in turn causes FCA on a low power continuous wave probe. The probe operates at 1549 nm and the pump at 1547 nm with a full-width at half maximum (FWHM) pulse duration of $t_{\mathrm{FWHM}} = 80$ ps and a repetition rate of 500 kHz. We used a variable optical attenuator to vary the pump peak power level coupled into the waveguide from 10 mW up to 1 W and, therefore, control the amount of generated carriers. By using pump pulses with the extinction ratio exceeding 30 dB, we avoid carrier generation between the pump pulses. In addition, by keeping the probe power at 50 μW, we ensure that the free-carrier density generated by the probe is negligible compared to that generated by the pump. Both the low probe power and the long repetition period of the pump pulses prevent carrier accumulation. The temporal traces were captured using a two-channel oscilloscope. One of the channels—an optical input with a 28 GHz built-in photodetector—was used to alternately measure the output probe and pump signals. The other channel—an electrical input with a 20 GHz external photodetector—was used to monitor the input pump pulses. In order to enhance the signal to noise ratio of the captured output probe, several traces were averaged, while making sure that the input pump power did not vary over the averaging process (the number of traces m was varied according to the pump power, for instance, $m = 75$ for 10 mW and $m = 5$ for 1 W).

Figure 1 shows the normalized time-resolved probe transmittance, $T(t)$, for three different pump powers: 100, 360, and 670 mW. Here, the normalized transmittance $T(t)$ is obtained by dividing the captured probe traces with pump-on and pump-off conditions, and therefore, it accounts only for losses induced by non-degenerate TPA and FCA. Two different regimes can be identified: an initial fast drop in the transmittance caused by non-degenerate TPA, followed by a slower regime where FCA is dominant. We measured the FCA loss at $t_0 = 100$ ps after the peak of the pulse (where non-degenerate TPA does not contribute), from which the generated carrier density can be obtained as[20,21]

$$\bar{N}(t_0) = -\frac{\ln[T(t_0)]}{S\sigma_r \eta L}, \tag{1}$$

where $\sigma_r = 1.45 \times 10^{-17}\,\mathrm{cm}^2$ is the FCA cross-section at 1550 nm[1,22] and η is the overlap factor between the optical mode and the silicon core. Given the short diffusion time ($\approx$10 ps), we calculated the overlap factor assuming a uniform carrier density in the core cross-section, resulting in $\eta = 0.77$ based on the Finite Element Method.[20] L is the waveguide length, and $S = 1.19$ is the slow-light factor that accounts for the decreased waveguide group velocity compared with bulk silicon, resulting in an FCA-enhancement.[23,24] It is important to note that $\bar{N}(t)$ stands for the longitudinally averaged carrier density, which for a short 2.4 mm-long waveguide represents well the local carrier density.[20] Figure 2 shows the generated carriers at t_0 to input peak power, $\bar{N}(t_0)/P_0$, for input pump peak power P_0 ranging from 10 to 100 mW. In this range, $\bar{N}(t_0)/P_0$ presents a clear linear dependence on P_0 with a non-zero intercept

$$\frac{\bar{N}(t_0)}{P_0} = a + bP_0. \tag{2}$$

By performing a linear regression, we obtain the coefficients $a = (0.9 \pm 0.1) \times 10^{13}\,\mathrm{cm}^{-3}\,\mathrm{mW}^{-1}$ and $b = (2.4 \pm 0.1) \times 10^{11}\,\mathrm{cm}^{-3}\mathrm{mW}^{-2}$. We now show that for low pump powers, where the FCA-induced pump depletion can be neglected, the coefficients a and b are directly related to α_{SPA} and β_{TPA}, the absorption coefficients due to SPA and TPA, respectively. As demonstrated by Aldaya *et al.*,[20] the dynamics of free-carriers can be highly nonlinear due to the trap-assisted recombination process. In particular, this process results in an instantaneous carrier lifetime that varies as recombination evolves (as a result of trap saturation). The instantaneous lifetime is shorter at the beginning of the recombination process and increases at later stages. This

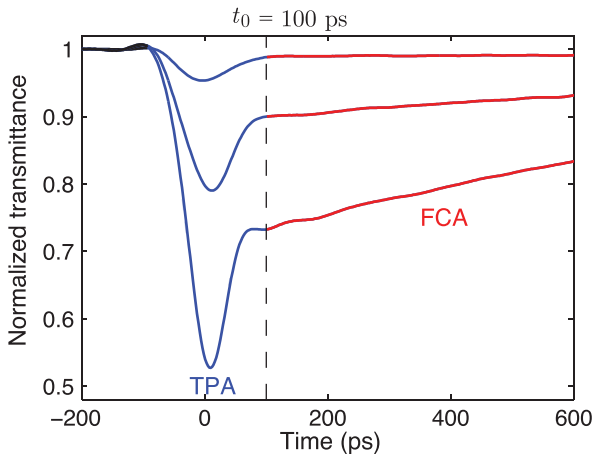

FIG. 1. Normalized probe transmittance for input pump powers of 100, 360, and 670 mW. The vertical line at $t_0 = 100$ ps represents the boundary between the regime dominated by non-degenerate TPA and the regime dominated by pure FCA.

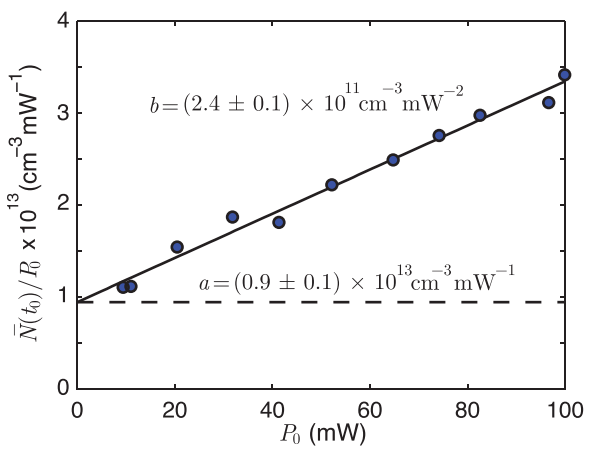

FIG. 2. Carrier density to power ratio in terms of the input pump power level up to 100 mW. The experimental data are presented alongside with the linear regression performed to extract the SPA and TPA coefficients.

represents a difficulty in extracting the absorption coefficient from continuous-wave measurements.[11] In our experiment, however, we measured the carrier density only 100 ps after the pump pulse, which allows us to use the shortest value for the carrier lifetime (for the waveguide under test, $\tau_c = 800$ ps as reported by Aldaya *et al.*[20]). As a result, the nonlinear recombination equations described by Aldaya *et al.*[20] can be simplified to the usual form

$$\frac{\partial N(z,t)}{\partial t} = g(z,t) - \frac{N(z,t)}{\tau_c}, \tag{3a}$$

$$g(z,t) = \frac{\alpha_{\mathrm{SPA}}}{\hbar\omega} I(z,t) + \frac{\beta_{\mathrm{TPA}}}{2\hbar\omega} I^2(z,t). \tag{3b}$$

The carrier generation rate $g(z, t)$ includes both SPA and TPA (recalling that we only consider free carriers generated by the pump signal), with $\hbar\omega$ being the photon energy, $I(z, t)$ the pump intensity, and z and t the spatial and temporal coordinates, respectively. In Eq. (3b), α_{SPA} and β_{TPA} correspond to the effective SPA and TPA coefficients, respectively. For relatively low pump power levels, pump depletion due to free carriers can be neglected, leading to an analytical expression for the pump intensity[24,25]

$$I(z,t) = \frac{I(0,t)\exp(-\alpha z)}{1 + \beta_{\mathrm{TPA}} I(0,t) L_{\mathrm{eff}}}, \tag{4}$$

where $I(0, t)$ is the pump intensity at the input of the waveguide, α stands for the linear propagation loss accounting for both scattering and SPA losses, and L_{eff} is the effective length (see Table I). In the low-power regime, the carrier generation rate $g(z, t)$ is independent of the carrier density itself, and therefore, Eq. (3a) is solved as

$$N(z,t) = e^{-\frac{t}{\tau_c}} \int_{-\infty}^{t} g(z,t') e^{\frac{t'}{\tau_c}} \mathrm{d}t'. \tag{5}$$

Since the measurements are taken at the end of the waveguide, we in fact observe the longitudinally averaged carrier density, $\bar{N}$, given by[20,21]

$$\begin{aligned} \bar{N}(t) &= \frac{1}{L}\int_0^L N(z,t)\,\mathrm{d}z \\ &= e^{-\frac{t}{\tau_c}} \int_{-\infty}^{t} \left[\frac{1}{L}\int_0^L g(z,t)\,\mathrm{d}z\right] e^{\frac{t'}{\tau_c}}\,\mathrm{d}t'. \end{aligned} \tag{6}$$

TABLE I. List of expressions.

Symbol	Expression
L_{eff}	$\frac{1-\exp(-\alpha z)}{\alpha}$
$L_{eff,2}$	$\frac{1-\exp(-2\alpha z)}{2\alpha}$
$\bar{I}(t)$	$I(0,t)\frac{L_{\mathrm{eff}}}{L}\left[1 - \frac{\beta_{\mathrm{TPA}} I(0,t) L_{\mathrm{eff}}}{2}\right]$
$\overline{I^2}(t)$	$I^2(0,t)\frac{L_{\mathrm{eff},2}}{L}$
$\tau_n[n=1,2]$	$\int_{-\infty}^{0} \exp\left(-\frac{nt^2}{2\sigma^2}\right)\exp\left(\frac{t}{\tau_c}\right)\mathrm{d}t$
a	$\frac{2\alpha_{\mathrm{SPA}}\tau_1}{\hbar\omega A_{\mathrm{eff}}}\frac{L_{\mathrm{eff}}}{L}\exp\left(\frac{-t_0}{\tau_c}\right)$
b	$\frac{\beta_{\mathrm{TPA}}\tau_2}{\hbar\omega A_{\mathrm{eff}}^2}\left(\frac{L_{eff,2}}{L} - \frac{\alpha_{\mathrm{SPA}} L_{\mathrm{eff}}^2}{L}\right)\exp\left(\frac{-t_0}{\tau_c}\right)$

This expression involves taking the spatial average of the generation rate $g(z, t)$, which based on Eq. (3b) requires taking the spatial average of the intensity $\bar{I}(t) = (1/L)\int_0^L I(z,t)\,\mathrm{d}z$ and of its square $\overline{I^2}(t) = (1/L)\int_0^L I^2(z,t)\,\mathrm{d}z$. Using Eq. (4), these averages can be calculated analytically leading, however, to cumbersome expressions. We therefore present in Table I the results for $\bar{I}(t)$ and $\overline{I^2}(t)$ only up to second order in the input intensity $I(0, t)$, which we verified to be valid in the power range in Fig. 2. With that, the carrier density from Eq. (6), evaluated at $t = t_0$, becomes

$$\bar{N}(t_0) = e^{-\frac{t_0}{\tau_c}} \int_{-\infty}^{t_0} \left[\frac{\alpha_{\mathrm{SPA}}}{\hbar\omega}\bar{I}(t') + \frac{\beta_{\mathrm{TPA}}}{2\hbar\omega}\overline{I^2}(t')\right] e^{\frac{t'}{\tau_c}}\,\mathrm{d}t'. \tag{7}$$

Using the expressions for $\bar{I}(t)$ and $\overline{I^2}(t)$ in Table I, the remaining time integration in Eq. (7) is easily performed assuming a Gaussian input pulse $I(0,t) = I_0 \exp(-t^2/2\sigma^2)$, with I_0 its peak intensity and $t_{\mathrm{FWHM}} = 2\sigma\sqrt{2\ln 2}$. Implicit time convolutions in Eq. (7) for $I(0, t)$ and $I^2(0, t)$ lead to the definition of the time constants, τ_1 and τ_2, in Table I. For the measurement time t_0 verifying that $t_{\mathrm{FWHM}} < t_0 < \tau_c$, we have made the approximation that $\int_{-\infty}^{t_0} \exp(-nt^2/2\sigma^2)\exp(t/\tau_c)\mathrm{d}t \approx 2\int_{-\infty}^{0} \exp(-nt^2/2\sigma^2)\exp(t/\tau_c)\mathrm{d}t$ for $n = 1$ and 2. Finally, in most cases, it is convenient to express the carrier density not in terms of the intensity but in terms of the input peak power P_0, which is related to I_0 and the effective area A_{eff} through $P_0 = I_0 A_{\mathrm{eff}}$. We use the definition of the propagating mode effective area as[26,27] $A_{\mathrm{eff}} = (\int S_z da)^2/\int S_z^2 da \approx 0.11\ \mu\mathrm{m}^2$ (where S_z is the z-component of the mode Poynting vector). With that, the averaged carrier density $\bar{N}$ can be expressed as a function of input peak power P_0 as in Eq. (2), with coefficients a and b presented in Table I. Using the values obtained for a and b in the experimental fitting of Fig. 2 and the expressions in Table I, our measurements reveal a TPA coefficient of $\beta_{\mathrm{TPA}} = (1.5 \pm 0.1)$ cm/GW that is significantly higher than the values usually reported for bulk (0.4 – 1.2 cm/GW) at 1550 nm,[12–14] and an SPA coefficient of $\alpha_{\mathrm{SPA}} = (1.9 \pm 0.1)\ \mathrm{m}^{-1}$, equivalent to a linear loss of approximately 0.1 dB/cm.

To validate that the measured TPA and SPA coefficients correctly describe carrier generation for higher pump power levels, we compare the measured carrier densities with numerical results obtained by a 1D finite difference approximation.[24] Since the numerical modeling accounts for FCA-induced pump depletion, its accuracy is not limited to low power levels. Figure 3 shows the experimental data alongside with simulation results that consider both TPA and SPA, revealing that indeed the measured coefficients accurately describe the carrier generation up to 1 W. Figure 3 also shows simulation results accounting for each generation mechanism independently. By direct inspection, three different regions can be identified: (I) a low-power region where almost the totality of carriers is generated through SPA, and TPA can be disregarded; (II) a broad region where both mechanisms are significant; and (III) a high-power regime where TPA of the pump is dominant, with SPA being negligible. Even if the power ranges defining each region are subjective and dependent on the particular application, we include two delimiters (discontinuous vertical lines) in

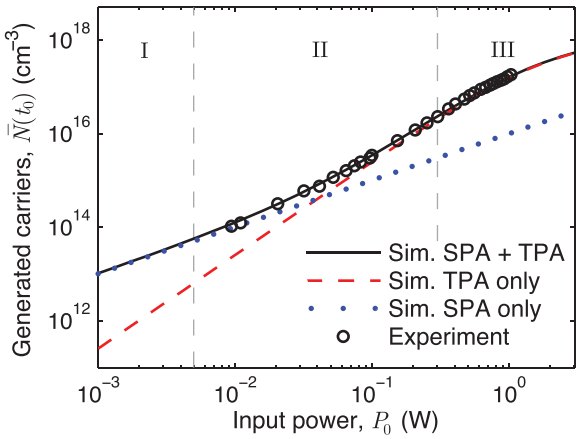

FIG. 3. Measured and calculated carrier density in terms of the input peak power (coupled into the waveguide). Simulation results considering SPA and TPA, TPA only, and SPA only.

Fig. 3(a) corresponding to the power levels at which 90% of the total carriers are generated assuming SPA only (∼5 mW) and TPA only (∼300 mW).

Both the low-power analytical approach and extended-range numerical simulations lead to a TPA coefficient that is higher than the value typically reported for bulk silicon at 1550 nm. In order to further confirm that such a high TPA coefficient is not a consequence of an error in the estimation of the pump power level coupled into the waveguide, we performed pump transmittance measurements in both directions, which are shown in Fig. 4. On the one hand, the good agreement between forward and backward transmittances is notable, verifying that both input and output coupling losses were correctly accounted for.[18] On the other hand, the measured TPA and SPA coefficients explain correctly the power depletion experienced by the pump, as can be seen from the matching between simulation and experimental results.

There are two key observations from our experiments: first, an increased value of the effective TPA coefficient of the guiding structure with respect to bulk; and, second, a non-negligible SPA that is important not only at very low power levels but also at moderate powers. An enhanced effect of TPA has been observed in photonic crystal

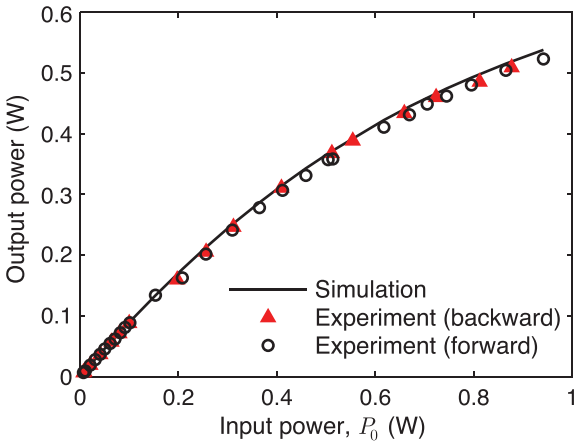

FIG. 4. Pump output peak power (before output grating) in terms of input peak power for backward and forward transmission. Simulation results considering $\beta_{TPA} = 1.5$ cm/GW and $\alpha_{SPA} = 1.9$ m^{-1}.

waveguides with very low group velocities,[24,28] and an elevated value of the TPA coefficient has also been measured in nano-waveguides, however only for wavelengths longer than 1775 nm.[19] Theoretically, several previous works have discussed the enhancement of nonlinearity in tight confinement waveguide structures.[23,26,27,29,30] In particular, Afshar *et al.*[27] discuss how this enhancement can be understood in terms of the material's nonlinear coefficients (suitably averaged over the waveguide cross-section), the mode's group velocity, and the definition of the effective area (either in terms of the Poynting vector area, which we used here, or in terms of the electric field intensity area—these two definitions being related implicitly by the group velocity). Taking these effects into account, theoretically, the nonlinearity enhancement relative to bulk is ≈20%. Our observation of $\beta_{\mathrm{TPA}} = (1.5 \pm 0.1)$ cm/GW is therefore in agreement with the high-end of the values previously reported in bulk or in much larger cross-section waveguides,[12–17] which are between 0.4 and 1.2 cm/GW for 1550 nm.

In conclusion, we simultaneously characterized linear and nonlinear optical carrier generation at 1550 nm in silicon fully etched nano-waveguides with silicon dioxide cladding. Pump-and-probe experiments reveal a TPA coefficient as high as (1.5 ± 0.1) cm/GW and an SPA coefficient of (1.9 ± 0.1) m^{-1}. The combination of an elevated effective TPA and non-negligible SPA leads to carrier densities larger than expected, which can have a significant impact on devices and phenomena based on free-carrier effects in silicon photonics. Furthermore, the experiments show that, at this wavelength window, carrier generation via SPA cannot be neglected up to ∼300 mW.

This work was supported by the São Paulo Research Foundation (FAPESP) (Nos. 2008/57857, 2012/50259-8, 2013/20180-3, and 2015/04113-0); the National Council for Scientific and Technological Development (CNPq) (No. 574017/2008-9); and the Coordination for the Improvement of Higher Education Personnel (CAPES).

[1]Q. Lin, O. J. Painter, and G. P. Agrawal, Opt. Express **15**, 16604 (2007).
[2]M. A. Foster, A. C. Turner, J. E. Sharping, B. S. Schmidt, M. Lipson, and A. L. Gaeta, Nature **441**, 960 (2006).
[3]T. Liang and H. Tsang, Appl. Phys. Lett. **84**, 2745 (2004).
[4]W. H. Pernice, M. Li, and H. X. Tang, Opt. Express **18**, 18438 (2010).
[5]I. Aldaya, A. Gil-Molina, H. L. Fragnito, and P. Dainese, in *Conference on Lasers and Electro-Optics* (CLEO) (IEEE, 2016), pp. 1–2.
[6]V. R. Almeida, C. A. Barrios, R. R. Panepucci, and M. Lipson, Nature **431**, 1081 (2004).
[7]L. Fan, J. Wang, L. T. Varghese, H. Shen, B. Niu, Y. Xuan, A. M. Weiner, and M. Qi, Science **335**, 447 (2012).
[8]D. Dimitropoulos, R. Jhaveri, R. Claps, J. Woo, and B. Jalali, Appl. Phys. Lett. **86**, 071115 (2005).
[9]J. J. Ackert, A. S. Karar, D. J. Paez, P. E. Jessop, J. C. Cartledge, and A. P. Knights, Opt. Express **21**, 19530 (2013).
[10]F. Morichetti, S. Grillanda, M. Carminati, G. Ferrari, M. Sampietro, M. J. Strain, M. Sorel, and A. Melloni, IEEE J. Sel. Top. Quantum Electron. **20**, 292 (2014).
[11]S. Grillanda and F. Morichetti, Nat. Commun. **6**, 8182 (2015).
[12]A. D. Bristow, N. Rotenberg, and H. M. van Driel, Appl. Phys. Lett. **90**, 191104 (2007).
[13]Q. Lin, J. Zhang, G. Piredda, R. W. Boyd, P. M. Fauchet, and G. P. Agrawal, Appl. Phys. Lett. **91**, 021111 (2007).
[14]M. Dinu, F. Quochi, and H. Garcia, Appl. Phys. Lett. **82**, 2954 (2003).

[15]H. K. Tsang, C. Wong, T. Liang, I. Day, S. Roberts, A. Harpin, J. Drake, and M. Asghari, Appl. Phys. Lett. **80**, 416 (2002).
[16]G. W. Rieger, K. S. Virk, and J. F. Young, Appl. Phys. Lett. **84**, 900 (2004).
[17]R. Claps, D. Dimitropoulos, V. Raghunathan, Y. Han, and B. Jalali, Opt. Express **11**, 1731 (2003).
[18]A. R. Motamedi, A. H. Nejadmalayeri, A. Khilo, F. X. Kärtner, and E. P. Ippen, Opt. Express **20**, 4085 (2012).
[19]X. Liu, J. B. Driscoll, J. I. Dadap, R. M. Osgood, S. Assefa, Y. A. Vlasov, and W. M. Green, Opt. Express **19**, 7778 (2011).
[20]I. Aldaya, A. Gil-Molina, J. L. Pita, L. H. Gabrielli, H. L. Fragnito, and P. Dainese, Optica **4**, 1219 (2017).
[21]H. Tsang, P. Snow, I. Day, I. White, R. Penty, R. Grant, Z. Su, G. Kennedy, and W. Sibbett, Appl. Phys. Lett. **62**, 1451 (1993).
[22]R. Soref and B. Bennett, IEEE J. Quantum Electron. **23**, 123 (1987).
[23]C. Monat, B. Corcoran, D. Pudo, M. Ebnali-Heidari, C. Grillet, M. D. Pelusi, D. J. Moss, B. J. Eggleton, T. P. White, and L. O'Faolain, IEEE J. Sel. Top. Quantum Electron. **16**, 344 (2010).
[24]Y. Zhang, C. Husko, S. Lefrancois, I. H. Rey, T. F. Krauss, J. Schröder, and B. J. Eggleton, Opt. Express **23**, 17101 (2015).
[25]L. Yin and G. P. Agrawal, Opt. Lett. **32**, 2031 (2007).
[26]S. Afshar V and T. M. Monro, Opt. Express **17**, 2298 (2009).
[27]S. Afshar V, T. M. Monro, and C. M. de Sterke, Opt. Express **21**, 18558 (2013).
[28]K. Kondo and T. Baba, Optica **4**, 1109 (2017).
[29]H. Kogelnik, "Integrated optics," in *Topics in Applied Physics*, edited by T. Tamir (Springer-Verlag, Berlin, 1975), Vol. 7, Chap. 2, pp. 13–81.
[30]R. Osgood, N. Panoiu, J. Dadap, X. Liu, X. Chen, I.-W. Hsieh, E. Dulkeith, W. Green, and Y. Vlasov, Adv. Opt. Photonics **1**, 162 (2009).